Synthesis and dissolution behaviour of CaO/SrO-containing sol-gel-derived 58S glasses.

Anthony L. B. Maçon[2,3,+ *], Sungho Lee[1,4,#] , Gowsihan Poologasundarampillai[5], Toshihiro Kasuga[1], Julian R. Jones[3,*]

[1] Division of Advanced Ceramics, Graduate School of Engineering,
Nagoya Institute of Technology
Gokiso-cho, Showa-ku, Nagoya 466-8555, Japan

[2] Frontier Research Institute for Materials Science, Nagoya Institute of Technology,
Gokiso-cho, Showa-ku, Nagoya 466-8555, Japan

[3] Department of Materials, Imperial College London,
South Kensington Campus, London SW7 2AZ, UK

[4] Division of Materials and Manufacturing Science, Graduate School of Engineering,
Osaka University,
2-1 Yamadaoka, Suita, Osaka 565-0871, Japan

[5] School of Materials, The University of Manchester,
Oxford Road, Manchester M13 9PL, UK

S. Lee is now with the Division of Material and Manufacturing Science, Osaka University.

+ A.L.B. Maçon is now with the Frontier Research Institute for Materials Science, Nagoya Institute of Technology.

* Corresponding author *E-mail address*: julian.r.jones@imperial.ac.uk,
alb.macon@nitech.ac.jp

Abstract

The effect of the substitution of strontium for calcium in the tertiary the SiO_2-CaO-P_2O_5 sol-gel bioactive glass 58S ($60SiO_2 \cdot 36CaO \cdot 4P_2O_5$, mol%) on its structure and its chemical durability on soaking in simulated body fluids was investigated. 58S was selected as a starting composition and substitution for calcium was carried out from 0 to 100% with an increment of 25%. A novel phosphate source of diethylphosphatoethyltriethoxysilane (DEPETES), which consists of Si and P connected with ethylene group, was used in this work. XRD and FTIR showed that the gels obtained following drying at 130 °C had a typical sol-gel structure, where a continuous amorphous silica gel network and surface bound mineral salts of $Ca(NO_3)_2$ and $Sr(NO_3)_2$. Once the gels were heat stabilised to decompose nitrates and incorporate the cations into the network, samples containing Sr formed a strontium silicate crystalline phase. With increasing levels of Sr in the composition, the overall crystallinity of the glass-ceramic increased, while, at the maximum substitution of 100% SrO, macroscopic phase separation was observed, characterised by needle-like crystals of strontium apatite ($Sr_5(PO_4)_3OH$) and strontium silicate (Sr_2SiO_4) phases in addition to amorphous regions. Dissolution experiments in Tris buffered solution showed Sr successfully released into the media even though it existed as a crystalline phase in the glass-ceramic. Further, the

glass-ceramics induced nucleation and growth of carbonated hydroxyapatite (HA) on their surface suggesting potential bioactivity of the materials. At higher substitutions (75% and 100% SrO for CaO) HA nucleation was not found to occur this may have been due to low amount of phosphate released from the original glass-ceramic as a result of it being locked up in the strontium apatite phase.

Keywords

Biomaterials, Sol-gel, Silicate, Phosphate, Calcium, Strontium

1. Introduction

Larry Hench's discovery of Bioglass® revolutionised the field of biomaterials, introducing the concept of bioactive materials, and was his first seminal discovery [1]. He also introduced the concept of sol-gel derived bioactive glasses.[2] His third seminal discovery was the key aspect of bioactive glasses, their ability to give chemical cues to surrounding cells, to either enhance their metabolism and accelerate the healing of the damaged broken bone or wounded skin, or trigger apoptosis in cancerous tissues [3-5]. In bioactive glasses (BG), chemical cues are produced by the release of inorganic ions from the glasses, which represents an exciting and safer alternative to conventional organic drugs such as BMPs. For instance, soluble silica was shown to be important for bone regeneration, increasing significantly the expression of collagen type I, up-regulating the expression of growth factors key to vascularization and inhibiting the osteoclastic activity [6-9]. Phosphate can stimulate the expression of matrix Gla protein, which plays a significant role in the organization of bone tissues [10], while calcium can activate cell receptors triggering the production of growth factors for bone regeneration [10-13]. These therapeutic ions can be released upon hydrolytic degradation of BGs. Efforts are currently being made in the field of medical glasses to i) understand the effect of ions on different cell/tissue types; ii) tailor the release of these ions by

correlating dissolution behaviours to glass structures.

With this mindset, strontium has been incorporated into bioactive glasses as it has multiple benefits for the regeneration of hard tissues. In the presence of Sr^{2+} ions, osteoblast metabolism is increased due to activation of calcium-sensing receptors [12,14-16]. In addition, 0.1 to 1 mM of Sr^{2+} ions enhances the alkaline phosphatase (ALP) activity, which is a marker for osteoblast differentiation, but inhibits osteoclast differentiation [17-19]. Multiple reports have described the incorporation of strontium in bioactive glasses, especially in their sol-gel derived form, from either a binary (SiO_2-CaO) [20-24] or ternary (SiO_2-P_2O_5-CaO) [25-32] systems, with the common denominator of substituting calcium for strontium.

However, the majority of these attempts only carried out partial substitution, making it difficult to appreciate the full impact of the substitution on the glass network and the resulting ability to release therapeutic cues. Nonetheless, Taherkhani *et al.* [32] reported the gradual and full substitution of calcium for strontium in 58S ($60SiO_2$-$36CaO$-$4P_2O_5$, mol%) sol-gel glass system, highlighting the impact on structure and mesoporosity. Upon substitution (5-100%), strontium silicate (Sr_2SiO_4) crystallized, suggesting that strontium cannot diffuse within the silica network as calcium does, which could hinder the delivery of strontium and silicate ions into body

fluids. However, they did not carry out a dissolution study, which is one of the main focus of the present manuscript. Here, strontium containing 58S bioactive glasses (substituted for calcium from 0% to 100%) were immersed in Tris buffered solution and simulated body fluid to evaluate the effect of the Sr_2SiO_4 crystallization onto their dissolution behaviour and the ability to surface nucleate calcium-phosphate crystals, respectively. Structural characterization was also conducted to affirmatively correlate the dissolution behaviour to the obtained structures. In addition, the present manuscript employs a phosphonate ester precursor in an attempt to reduce the tendency to form strontium apatite crystals, as orthophosphate is required for the formation of apatite.

2. Materials and methods

2.1. Synthesis of the glasses

Strontium-containing 58S ($60SiO_2 \cdot 36CaO \cdot 4P_2O_5$, mol%) were prepared with tetraethylorthosilicate (TEOS, Sigma-Aldrich), calcium nitrate tetrahydrate ($Ca(NO_3)_2 \cdot 4H_2O$, Sigma-Aldrich), strontium nitrate ($Sr(NO_3)_2$, Sigma-Aldrich) and diethylphosphatoethyltriethoxysilane (DEPETES, fluorochem), using the sol-gel process. Nominal compositions of the glasses are given in Table 1: the sample code denoted as *x*Sr, and *x* means SrO substitution ratio (%). TEOS and distilled water were

placed in a polytetrafluoroethylene (PTFE) container at a H_2O:TEOS molar ratio of 12:1 and mixed for 5 minutes. 2 M nitric acid (HNO_3) was used as a catalyst and added to the sol at H_2O:HNO_3 volume ratio of 6:1 [33]. The resulting solution was vigorously mixed for 1 h, at room temperature, to ensure complete hydrolysis of TEOS. DEPETES was then added and mixed for 1 h followed by the addition of calcium nitrate and strontium nitrate and a further mixing of 1 h. The containers were then sealed (screw top) and the sol aged at 60 ºC for 72 h (sealed PTFE container). The obtained gels were dried by loosening the screw top in a sequential program starting at 60 ºC (20 h), then going at 90 ºC (24 h) and 130 ºC (40 h) with heating rate 0.1 ºC/min. The dried gels were thermally stabilized using a sequential program of 100 ºC (5 min) with heating rate 1 ºC/min, then at 300 ºC (2h) with heating rate 0.5 ºC/min and 700 ºC (5 h) with heating rate 1 ºC/min, and then cooling down to room temperature with cooling rate 5 ºC/min.

2.2. Glass composition

The resulting glass compositions were examined using inductivity coupled plasma optical emission spectroscopy (ICP-OES, Thermo iCAP, Thermo scientific): 25 mg of the glass powders and 125 mg of $LiBO_2$-$Li_2B_4O_7$ (80:20 w/w%, Spectroflux® 100B, Alfa Aesar) were mixed and heat-treated for 10 min at 950 ºC in platinum

crucible, and the resulting mixture were dissolved 100 mL of 2 M HNO_3 and then the solution evaluated by ICP-OES.

2.3. Characterisation of the glass structures

Before and after stabilisation, glasses were examined by attenuated total reflectance Fourier transform infrared spectroscopy (FTIR, Nicolet iS10, Thermo scientific), focusing on the spectral range from 400 to 1600 cm^{-1} with scan number of 50; and powder X-ray diffraction (XRD, X'pert-MPD, PANalytical) with 2θ ranging from 10º to 40º with scan speed 0.04 º/s. Non-stabilized glasses were examined by thermogravimetry differential thermal analysis (TG-DTA, heating rate: 5 K/min, Thermoplus TG8120, Rigaku).

2.4. Characterisation of dissolution to Tris buffer solution and simulated body fluids

Tris buffer solution (TBS) was prepared according the procedure, 15.090 g of tris-(hydroxymethyl)aminomethane (VMR Chemicals) was dissolved in 2000 mL of deionized water, and the pH adjusted to 7.30 with 1 M hydrochloric acid. 100 mg of glass powder was immersed in 150 mL of TBS and agitated at 120 rpm using orbital shaker at 37 ºC [34]. Aliquots of 1 mL were taken and replaced with 1 mL fresh TBS at

1, 2, 4, 8, 24, 72, 120, 168 and 336 h. The aliquots were then diluted 10 times using 2 M HNO_3 and subsequently measured using ICP-OES. Samples soaked in TBS for 336 h were filtered and dried at 37 ºC, and examined using FTIR, XRD and SEM (LEO Gemini 1525, ZEISS). Simulated body fluid (SBF) was prepared following the method of Kokubo *et al.* [35] and dissolution test process as that with TBS was conducted.

3. Results and discussion

Strontium-containing 58S ($60SiO_2 \cdot (36–x)CaO \cdot 4P_2O_5 \cdot xSrO$, mol%) were synthesised here with different degrees of calcium to strontium substitution from 0 to 100 % (*e.g.* x = 0 to x = 36) with a gradual increase of 25 %, namely 0Sr, 25Sr, 50Sr, 75Sr and 100Sr, corresponding to x = 0, 9, 18, 27 and 36 respectively. Details of the nominal compositions of the glasses are given in Table 1. Before evaluating the effect of Sr substitution on the dissolution behaviour, the evolution of the glass structure upon heat stabilisation was studied using FTIR, XRD, SEM and TG-DTA.

3.1. Glass structure

3.1.1. Before heat stabilisation

After drying the glasses, no phase separation could be observed. XRD and

FTIR were performed on the dried gels as shown in Fig. 1. All FTIR spectra revealed bands characteristic of a dried bioactive sol-gel glass prepared with mineral salts, with: i) vibrational features of silicon bridging oxygen (Si-O-Si) at $\mathbf{v}_{\text{Si-O-Si,ro}} \approx 430$ cm^{-1} in rocking mode [36], $\mathbf{v}_{\text{Si-O-Si,ben}} \approx 780$ cm^{-1} in bending mode [36] and $\mathbf{v}_{\text{Si-O-Si,stret}}$ from 1000 to 1300 cm^{-1} in asymmetric stretching mode both optically transverse and longitudinal resonant mode were observed [36-38]. The Si-O stretching mode of non-bridging oxygen atoms (NBO) could be observed at 951 cm^{-1}, originating from the free silanol present on the surface of the mesopores or silicate moieties that stabilised calcium or strontium within the silica network [36,38]; ii) vibration characteristic of nitrate (NO_3^-) in a crystalline form were also observed, with broad bands between 1250 and 1500 cm^{-1} and sharp bands at 815 and 738 cm^{-1} [33,39,40]. The presence of mineral salts was confirmed by the XRD as shown in Fig. 1 (b). 0Sr displayed diffraction peaks characteristic of $Ca(NO_3)_2{\cdot}4H_2O$ (ICCD card: 26-1406), while a mixture of $Ca_{0.33}Sr_{0.67}(NO_3)_2$ (ICCD card: 26-1073) and calcium nitrate was observed with 25Sr and 50Sr. Strontium nitrate, $Sr(NO_3)_2$ (ICCD card: 76-1375), was the only crystalline phase detected above 50% of calcium substitution.

The observations made here by XRD and FTIR were in line with previous structural characterisations of bioactive glasses synthesized by the sol-gel process using

mineral salts as cation precursors. For instance, Lin *et al.* demonstrated, with a binary system of silica and calcium, that calcium nitrate redeposits onto the surface of silica secondary particles upon drying of the gel [41]. Calcium diffused within the silica network, through the breaking of bridging oxygen, upon heat stabilisation above 450 ºC. Similar observations were made for binary systems composed of silica and strontium, where $Sr(NO_3)_2$ precipitated upon drying [42]. Structural characterization performed on similar compositions to these reported here suggests that an acidic catalysed (below the pKa of silicic acid) sol-gel process favours the formation of silanol (Si-OH) as opposed to silicate ($Si\text{-}O^-$), enhancing the precipitation of mineral salt [28].

In order to yield nitrate-free bioactive glasses, the dried gels must be heat stabilised [41]. The stabilisation temperature was selected based on the TG-DTA measurement shown in Fig. 2, where 0Sr and 100Sr are displayed. TG-DTA traces of 25Sr, 50Sr and 75Sr are shown in the supplementary information (Fig. S1). The residual mass for 0Sr decreased quasi-steadily from 200 ºC to 550 ºC, whereas a sharp weight loss was observed for 100Sr around 580 ºC. From the DTA traces, 0Sr and 100Sr showed exothermic peaks between 200 ºC and 400 ºC, corresponding to a weight loss 25% and 6%, respectively, and caused by restricted dehydration of the nitrate salt, along with the dehydroxylation of vicinal silanols [43,44]. The weight loss of 0Sr was more

pronounced than 100Sr, as 0Sr contained hydrated $Ca(NO_3)_2$, as shown by XRD (Fig. 1. (b)). In addition, it is likely that the presence of water in the $Ca(NO_3)_2$ structure induced a more gentle decomposition/evaporation of the nitrate counter ions, supported by the water desorption, which in turn favoured the diffusion of calcium ions within the silica [41]. Taherkhani *et al.* also reported an increased and more drastic weight loss with fully substituted dried gels [28]. The hypothesis made above could also explain why the onset endothermic peak generated by the decomposition of nitrate was lower for 0Sr (~550 ºC) than for 100Sr (~610 ºC). A stabilisation temperature of 700 ºC was selected for heat stabilisation, as nitrate was fully decomposed/evaporated at this temperature regardless of the compositions.

3.1.2. Post heat stabilisation

After heat stabilisation, no macroscopic phase separation was observed, except when calcium was fully substituted for strontium (100Sr), which had a mix of particle morphologies. 100Sr was manually separated into needle-like ($100Sr_{needle\text{-}like}$) and glassy ($100Sr_{glassy}$) particles, extracting the macroscopic needles using tweezers, and their compositions analysed (Table 2). SEM, FTIR and XRD analysis were performed on the collected powders as shown in Fig. 3 (a-d). From the infrared measurements,

$100Sr_{needle\text{-}like}$ showed all the characteristics of a silicate containing crystalline lattice with sharp Si-O NBO bands between 800 to 1000 cm^{-1}. While, the Si-O-Si asymmetric stretching band at 1074 cm^{-1} was the dominating vibration in $100Sr_{glassy}$, indicating that the main phase was composed of an amorphous silica network. These observations were corroborated by the XRD measurements as shown in Fig. 3 (d). The $100Sr_{glassy}$ samples had an amorphous halo centred around 22 º 2θ with low diffraction peaks from strontium silicate Sr_2SiO_4 (ICCD card: 76-1630), while only strong diffraction peaks from Sr_2SiO_4 and strontium apatite $Sr_5(PO_4)_3OH$ (ICCD card: 33-1348) were observed for 100Sr needle-like. Since the glassy and crystalline phases could not be completely manually separated, the glass-ceramic composite was mixed ground together for dissolution tests.

Structural characterizations (FTIR and XRD) were also performed on the other stabilized gels as shown in Fig. 4. According to the FTIR measurements, nitrate-free samples were obtained, regardless of the compositions, confirming that 700 ºC was an adequate temperature for heat stabilization. The FTIR spectrum from 58S (0Sr) was in agreement with previous report, with absorption bands characteristic of an amorphous silica network (as described above for non-stabilized samples) [45]. Similar bands were observed with 25% of substitution. However, at 50Sr and above, noticeable and gradual

variations could be seen, with an increase in absorption from the silicon non-bridging oxygen, at 951 cm^{-1}, as the degree of substitution increased, characteristic of the devitrification of sol-gel glasses [46]. In addition, bands characteristic of the bending mode of phosphate (P-O) in a crystal lattice at 567 and 597 cm^{-1} [42], along with the vibration of carbonate species (CO_3^{2-}) at 710 and 1467 cm^{-1} could be observed. [36]. This suggests that glass-ceramics with strontium apatite as a crystalline phase were produced from 50% of calcium to strontium substitution and was confirmed by XRD as shown in Fig. 4 (b). Diethylphosphatoethyltriethoxysilane (DEPETES), an organo-phosphonosilane, was used in this work as a phosphate source instead of the conventional triethylphosphate (TEP) in order to prevent the formation of apatite crystal during stabilization [32,47]. It appears that the carbon bridge of DEPETES decomposed at low temperature, generating phosphite residues, which then underwent oxidation with the surrounding oxygen (heat stabilisation in air) to orthophosphate. In addition to the precipitation of apatite, peaks characteristic to strontium silicate were also detected using XRD at 50Sr and above with a gradual increase in intensity as the amount of strontium increased in the samples. Finally, the actual compositions of the heat-stabilised gels were in relatively good agreement with the nominal as shown in Table 2.

From the observations, along with the TG-DTA data, we can hypothesise that the difference in crystallization of the calcium and strontium with the other elements present is primarily due to the difference in decomposition of their nitrate counterpart during heat stabilization; The rapid decomposition of strontium nitrate produced a higher concentration of strontium in the mesopores compared to calcium, which gradually diffused in the silica network. At this stage of the stabilisation, the thermal energy is high enough that strontium ions charged balance with silicates via a heterogeneous crystallisation where the silanols present at the mesopores acted as nucleation sites [48]. However, it was not possible to confirm this hypothesis.

3.2. Dissolution behaviour and apatite forming ability in Tris buffered solution and SBF.

In order to evaluate whether the crystallization of the gels containing strontium had impaired the dissolution behaviour, the glasses and glass-ceramics were immersed in Tris buffered solution (TBS). Since part of the phosphate crystallized into strontium apatite during heat stabilization, the release of phosphorus was expected to be low or below the detection limit of ICP-OES (P_2O_5 only represents 4 mol% of the composition in 58S). Thus, TBS was selected as media as it does not contain any ions, facilitating the

monitoring of the phosphate release.

The concentration profiles of silicate, phosphate, calcium and strontium upon immersion in TBS over 2 weeks are shown in Fig. 5 (a). The silicate dissolution behaviour showed no significant difference between the samples, with a rapid increase in its concentration within the first two days, then plateauing off. The initial silicate ion release rate was 0.09 mM/h, leading to a total released of 2.1 ± 0.02 mM after 336 h of immersion, regardless of the compositions.

The release profiles of phosphorus depended on the composition. The amount of P released from 0Sr, 25Sr and 50Sr increased within the first 8 h, with initial release rate of 0.13 mM/h, 0.07 mM/h and 0.03 mM/h, respectively. Then, a decline in concentration was observed with increasing soaking time, and indicated 0 mM after 24 h, 72 h and 120 h of immersion for 0Sr, 25Sr and 50Sr, respectively, suggesting the precipitation/nucleation of phosphate-containing phase. The amount of P released in TBS from 75Sr and 100Sr increased up to 24 h at a rate of 0.018 and 0.005 mM/h and stood constant with concentration of 0.43 ± 0.02 and 0.13 ± 0.01 mM, respectively. The fact that P was released from all the compositions suggests that phosphate residues only partially devitrified to form $Sr_5(PO_4)_3OH$ during the heat stabilization.

The release of calcium and strontium were in proportion to the nominal

composition of the stabilized gels and followed the same trends. The initial release rate of Ca ions decreased as the degree of substitution increased, from 0.79 mM/h for 0Sr to 0.09 mM/h for 75Sr, while the opposite trend was observed for Sr, with initial rates going from 0.19 mM/h for 25Sr to 0.80 mM/h for 100Sr. After 72h of soaking, the Ca and Sr concentration showed no significant variation with increasing soaking time, with values ranging from 4.98 ± 0.09 to 0.93 ± 0.07 mM for calcium and from 1.16 ± 0.03 to 5.44 ± 0.34 mM for strontium. Most of the strontium was present in the crystal form of strontium silicate (Sr_2SiO_4). To our knowledge, the solubility constant of Sr_2SiO_4 has never been published. The ICP-OES data presented in this report suggests that this crystal is highly soluble, allowing for the release of strontium in solution, regardless of the dissolution condition used. However, it is not possible to know whether strontium was released as ions or as nanocrystal of Sr_2SiO_4.

The surfaces of the samples after 2 weeks of immersion were analyzed by XRD, FTIR and SEM as shown in Fig. 5 (c) and (d) and Fig. 6. The hypothesis made on the solubility of Sr_2SiO_4 was reinforced by the surface analysis with a drastic decrease of the intensity of the silica NBO in FTIR (Sr_2SiO_4 contains only silica NBO), as compared to the samples before immersion, and the absence of Sr_2SiO_4 diffraction peaks in XRD. Similarity between the samples were seen in FTIR with bands related to

vibration of silica networks (Si-O-Si at 454, 797, 1025 and 1218 cm^{-1}) [36,37,45], carbonates (CO_3^{2-} at 862-877 and 1410-1464 cm^{-1}) [36] and orthophosphate in crystalline phase (P-O in PO_4^{3-} at 564-600 cm^{-1}) [45] seen in all samples, usually indicating the surface nucleation of phosphate containing crystals. XRD measurement revealed that hydroxyapatite was present on 0Sr and 25Sr; while a mix of hydroxyapatite and strontium apatite was observed at 50Sr. Strontium apatite was the only phase detected for 75Sr and 100Sr. However, for 0Sr to 50Sr, SEM images showed needle-like crystals, which are characteristic of hydroxyapatite, formed as a result of a dissolution/nucleation mechanism (Fig. 6 (a-c)). Any strontium apatite formation was below detection limits for these compositions. In contrast, smooth surfaces were observed in SEM images of 75Sr and 100Sr (Fig. 6 (d-e)), which, in combination with the result that the TBS containing 75Sr and 100Sr did not decrease in phosphate concentration at any point, indicates that any precipitation of strontium apatite was below detection limits. The $Sr_5(PO_4)_3OH$ present in the XRD patterns of 75Sr and 100Sr was already present before the immersion from these compositions.

The stabilised gels were also immersed in simulated body fluid (SBF) for two weeks in order to investigate whether an increase in ionic strength of the media could result in an increase in the calcium phosphate nucleation for the sample with 50% of

substitution and above [49]. FTIR, XRD and SEM of collected powder after immersion are shown in Fig. 7. No differences were seen between the sample immersed in TBS and SBF in terms of surface analysis. Several reports on the dissolution behaviour of partially substituted sol-gel glasses (equivalent to 25Sr) described an increase in quality and speed of the nucleation of calcium-phosphate in SBF, compared to no strontium [25,50,51]. When fully substituted in melt-derived glass ($49.46SiO_2 \cdot 1.07P_2O_5 \cdot 23.08 \cdot SrO \cdot 26.38Na_2O$, in mol%), glass degradation and apatite formation was significantly increased [52,53]. Therefore, it is likely that the reduction in apatite formation at a high degree of substitution was not due to the release of strontium in solution but to devitrification of the glass upon heat stabilization, which as a result altered the surface chemistry of the samples.

4. Conclusions

Strontium-containing 58S were prepared using the sol-gel method employing a novel phosphate source. With increasing amounts of SrO substituted in the place of CaO, the materials showed phase separation with the formation of amorphous and crystalline phases, strontium apatite ($Sr_5(PO_4)_3OH$) and strontium silicate (Sr_2SiO_4). This indicated that the use of DEPETES did not suppress apatite formation, suggesting conversion of

phosphanate to orthophosphate during thermal stabilisation. TGA and XRD studies suggested that the devitrification that occurred during thermal stabilisation of the SrO substituted glasses may be explained by the rapid desorption of water from the $Sr(NO_3)_2$ upon heating, causing supersaturation of Sr within the mesopores of the gels leading to phase separation and crystallisation. Dissolution experiments showed, upon soaking the samples in Tris buffered solution (TBS) and SBF, the Sr_2SiO_4 peaks from the glass-ceramics dissolved out. Suggesting that the strontium silicate formed on devitrification of the glasses exhibited high solubility in simulated body fluids. Hydroxyapatite ($Ca_5(PO_4)_3OH$) precipitated on 0Sr, 25Sr and 50Sr samples in TBS indicating good bioactivity of 0Sr, 25Sr and 50Sr. Samples soaked in SBF for 336 h had formed $Ca_5(PO_4)_3OH$ on their surfaces while 25Sr, 50Sr, 75Sr and 100Sr had formed both $Ca_5(PO_4)_3OH$ and $Sr_5(PO_4)_3OH$.This suggests that both strontium apatite and hydroxyapatite had precipitated on their surfaces.

Acknowledgements

The authors would like to thank Engineering and Physical Sciences Research Council (GB, EP/I020861/1) and Japan Society for the Promotion of Science (JSPS) international training program for funding this project. Raw data is available on request

from alb.macon@nitech.ac.jp or julian.r.jones@imperial.ac.uk.

References

[1] Jones JR (2013) Review of bioactive glass: From Hench to hybrids, Acta Biomater. 9:4457-4486.

[2] Li R, Clark AE, Hench LL (1991) An investigation of bioactive glass powders by sol-gel processing, J. Appl. Biomater. 2:231.

[3] Hoppe A, Mourino V, Boccaccini AR (2013) Therapeutic inorganic ions in bioactive glasses to enhance bone formation and beyond, Biomater. Sci. 1:254-256.

[4] Hoppe A, Güldal NS, Boccaccini AR (2011) A review of the biological response to ionic dissolution products from bioactive glasses and glass-ceramics, Biomaterials 32:2757-2774.

[5] Thompson KH, Orvig C (2003) Boon and bane of metal ions in medicine, Science 300:936-939.

[6] Henstock JR, Canham LT, Anderson SI (2015) Silicon: The evolution of its use in biomaterials, Acta Biomater. 11:17-26.

[7] Mladenović Ž, Johansson A, Willman B, Shahabi K, Björn E, Ransjö M (2014) Soluble silica inhibits osteoclast formation and bone resorption in vitro, Acta Biomater. 10:406-418.

[8] Li H, Chang J (2013) Bioactive silicate materials stimulate angiogenesis in

fibroblast and endothelial cell co-culture system through paracrine effect, Acta Biomater. 9:6981-6991.

[9] Reffitt DM, Ogston N, Jugdaohsingh R, et al. (2003) Orthosilicic acid stimulates collagen type 1 synthesis and osteoblastic differentiation in human osteoblast-like cells in vitro, Bone 32:127-135.

[10] Julien M, Magne D, Masson M, et al. (2007) Phosphate stimulates matrix Gla protein expression in chondrocytes through the extracellular signal regulated kinase signaling pathway, Endocrinology 148:530-537.

[11] Julien M, Khoshniat S, Lacreusette A, et al. (2009) Phosphate-dependent regulation of MGP in osteoblasts: Role of ERK1/2 and Fra-1, J. Bone Miner. Res. 24:1856-1868.

[12] Marie PJ (2010) The calcium-sensing receptor in bone cells: A potential therapeutic target in osteoporosis, Bone 46:571-576.

[13] Valerio P, Pereira MM, Goes AM, Leite MF (2009) Effects of extracellular calcium concentration on the glutamate release by bioactive glass (BG60S) preincubated osteoblasts, Biomed. Mater. 4:045011.

[14] Marie PJ, Ammann P, Boivin G, Rey C (2001) Mechanisms of action and therapeutic potential of strontium in bone, Calcif. Tissue Int. 69:121-129.

[15] Marie PJ (2007) Strontium ranelate: New insights into its dual mode of action, Bone 40:S5-S8.

[16] Chattopadhyay N, Quinn SJ, Kifor O, Ye C, Brown EM (2007) The calcium-sensing receptor (CaR) is involved in strontium ranelate-induced osteoblast proliferation, Biochem. Pharmacol. 74:438-447.

[17] Barbara A, Delannoy P, Denis BG, Marie PJ (2004) Normal matrix mineralization induced by strontium ranelate in MC3T3-E1 osteogenic cells, Metabolism 53:532-537.

[18] Autefage H, Gentleman E, Littmann E, Hedegaard MAB, Von Erlach T, O'Donnell M, Burden FR, Winkler DA, Stevens MM (2015) Sparse feature selection methods identify unexpected global cellular response to strontium-containing materials, PNAS 112: 4280–4285.

[19] Takahashi N, Sasaki T, Tsouderos Y, Suda T (2003) S 12911-2 inhibits osteoclastic bone resorption in vitro, J. Bone Miner. Res. 18:1082-1087.

[20] Lao J, Jallot E, Nedelec J-M (2008) Strontium-delivering glasses with enhanced bioactivity: A new biomaterial for antiosteoporotic applications?, Chem. Mater. 20:4969-4973.

[21] Lao J, Nedelec JM, Moretto P, Jallot E (2008) Micro-PIXE–RBS methods

highlighting the influence of phosphorus on the in vitro bioactivity of sol–gel derived glass particles in the SiO_2–CaO–P_2O_5 system, Nucl. Instrum. Meth. B 66:2412-2417.

[22] Kim IY, Towler MR, Wren A, Ohtsuki C (2009) Fabrication of spherical CaO–SrO–ZnO–SiO_2 particles by sol–gel processing, J. Mater. Sci. Mater. Med. 20:2267-2273.

[23] Isaac J, Nohra J, Lao J, et al. (2011) Effects of strontium-doped bioactive glass on the differentiation of cultured osteogenic cells, Eur. Cells Mater. 21:130-143.

[24] Bonhomme C, Gervais C, Folliet N, et al. (2012) ^{87}Sr solid-state NMR as a structurally sensitive tool for the investigation of materials: Antiosteoporotic pharmaceuticals and bioactive glasses, J. Am. Chem. Soc. 134:12611-12628.

[25] Lao J, Nedelec JM, Jallot E (2009) New strontium-based bioactive glasses: physicochemical reactivity and delivering capability of biologically active dissolution products, J. Mater. Chem. 19:2940-2949.

[26] Hesaraki S, Gholami M, Vazehrad S, Shahrabi S (2010) The effect of Sr concentration on bioactivity and biocompatibility of sol–gel derived glasses based on CaO–SrO–SiO_2–P_2O_5 quaternary system, Mater. Sci. Eng. C 30:383-390.

[27] Zhu Y, Li X, Yang J, Wang S, Gao H, Hanagata N (2011) Composition-structure-property relationships of the CaO-M_xO_y-SiO_2-P_2O_5 (M = Zr,

Mg, Sr) mesoporous bioactive glass (MBG) scaffolds, J. Mater. Chem. 21:9208-9218.

[28] Taherkhani S, Moztarzadeh F, Mozafari M, Lotfibakhshaiesh N (2012) Sol–gel synthesis and characterization of unexpected rod-like crystal fibers based on SiO_2–(1-x)CaO–xSrO–P_2O_5 dried-gel, J. Non-Cryst. Solids 358:342-348.

[29] Wu C, Zhou Y, Lin C, Chang J, Xiao Y (2012) Strontium-containing mesoporous bioactive glass scaffolds with improved osteogenic/cementogenic differentiation of periodontal ligament cells for periodontal tissue engineering, Acta Biomater. 8:3805-3815.

[30] Zhang Y, Wei L, Chang J, et al. (2013) Strontium-incorporated mesoporous bioactive glass scaffolds stimulating in vitro proliferation and differentiation of bone marrow stromal cells and in vivo regeneration of osteoporotic bone defects, J. Mater. Chem. B 1:5711-5722.

[31] Dziadek M, Zagrajczuk B, Menaszek E, Wegrzynowicz A, Pawlik J, Cholewa-Kowalska K (2016) Gel-derived SiO_2–CaO–P_2O_5 bioactive glasses and glass-ceramics modified by SrO addition, Ceram. Int. 42:5842-5857.

[32] Taherkhani S, Moztarzadeh F (2016) Influence of strontium on the structure and biological properties of sol–gel-derived mesoporous bioactive glass (MBG) powder,

J. Sol-Gel Sci. Technol. 78:539-549.

[33] Saravanapavan P, Hench LL (2003) Mesoporous calcium silicate glasses. I. Synthesis, J Non-Cryst Solids 318:1-13.

[34] Maçon ALB, Kim TB, Valliant EM, et al. (2015) A unified in vitro evaluation for apatite-forming ability of bioactive glasses and their variants, J. Mater. Sci. Mater. Med. 26:1-10.

[35] Kokubo T, Kushitani H, Sakka S, Kitsugi T, Yamamuro T (1990) Solutions able to reproduce *in vivo* surface-structure changes in bioactive glass-ceramic A-W3, J Biomed Mater Res 24:721-734.

[36] Aguiar H, Serra J, González P, León B (2009) Structural study of sol–gel silicate glasses by IR and Raman spectroscopies, J. Non-Cryst. Solids 355:475-480.

[37] Sepulveda P, Jones JR, Hench LL (2001) Characterization of melt-derived 45S5 and sol-gel–derived 58S bioactive glasses, J. Biomed. Mater. Res. 58:734-740.

[38] Mozafari M, Moztarzadeh F, Rabiee M, et al. (2010) Development of macroporous nanocomposite scaffolds of gelatin/bioactive glass prepared through layer solvent casting combined with lamination technique for bone tissue engineering, Ceram. Int. 36:2431-2439.

[39] Irish DE, Walrafen GE (1967) Raman and infrared spectral studies of aqueous

calcium nitrate solutions, J. Chem. Phys. 46:378-384.

[40] Goebbert DJ, Garand E, Wende T, et al. (2009) Infrared spectroscopy of the microhydrated nitrate ions $NO_3^-(H_2O)_{1-6}$, J. Phys. Chem. A 113:7584-7592.

[41] Lin S, Ionescu C, Pike KJ, Smith ME, Jones JR (2009) Nanostructure evolution and calcium distribution in sol-gel derived bioactive glass, J. Mater. Chem. 19:1276-1282.

[42] Yamane M, Kojima T (1981) Low temperature synthesis of non-crystalline solids of the system $SrO–SiO_2$, J. Non-Cryst. Solids 44:181-190.

[43] Brinker CJ, Scherer GW (1990) Sol-gel science: The physics and chemistry of sol-gel processing, Academic Press, San Diego.

[44] Zhuravlev LT (2000) The surface chemistry of amorphous silica. Zhuravlev model, Colloids and Surfaces A: Physicochem. Eng. Aspects 173:1-38.

[45] Sepulveda P, Jones JR, Hench LL (2002) *In vitro* dissolution of melt-derived 45S5 and sol-gel derived 58S bioactive glasses, J. Biomed. Mater. Res. 61:301-311.

[46] Paluszkiewicz C, Blażewicz M, Podporska J, Gumuła T (2008) Nucleation of hydroxyapatite layer on wollastonite material surface: FTIR studies, Vib. Spectrosc 48:263-268.

[47] González B, Colilla M, Vallet-Regí M (2013) Design of in vitro bioactive hybrid

materials from the first generation of amine dendrimers as nanobuilding blocks, Chem. Eur. J. 19:4883-4895.

[48] Maçon ALB, Jacquemin M, Page SJ, et al. (2016) Lithium-silicate sol–gel bioactive glass and the effect of lithium precursor on structure–property relationships, J. Sol-Gel Sci. Technol. doi:10.1007/s10971-016-4097-x.

[49] Kokubo T, Takadama H (2006) How useful is SBF in predicting in vivo bone bioactivity?, Biomaterials 27:2907-2915.

[50] Hesaraki S, Alizadeh M, Nazarian H, Sharifi D (2010) Physico-chemical and in vitro biological evaluation of strontium/calcium silicophosphate glass, J. Mater. Sci. Mater. Med. 21:695-705.

[51] Shahrabi S, Hesaraki S, Moemeni S, Khorami M (2011) Structural discrepancies and in vitro nanoapatite formation ability of sol–gel derived glasses doped with different bone stimulator ions, Ceram. Int. 37:2737-2746.

[52] Fredholm YC, Karpukhina N, Brauer DS, Jones JR, Law RV, Hill RG (2012) Influence of strontium for calcium substitution in bioactive glasses on degradation, ion release and apatite formation, J. R. Soc. Interface 9:880-889.

[53] Padilla S, Román J, Carenas A, Vallet-Regí M (2005) The influence of the phosphorus content on the bioactivity of sol–gel glass ceramics, Biomaterials

1 26:475-483.

Figure and table captions

Figure 1: (a) FT-IR spectra and (b) XRD patterns of non-stabilized glasses.

Figure 2: TG-DTA traces of non-stabilized 0Sr and 100Sr.

Figure 3: SEM images of (a) $100Sr_{needle\text{-}like}$ and (b) $100Sr_{glassy}$, and (c) FT-IR spectra and (d) XRD patterns of 100Sr, $100Sr_{needle\text{-}like}$ and $100Sr_{glassy}$.

Figure 4: (a) FT-IR spectra and (b) XRD patterns of stabilized glasses. (eg. Dash line: TGA, plain: DTA)

Figure 5: (a) Ions concentration in TBS after soaking the glasses, and (b) FT-IR spectra and (c) XRD patterns of the glasses after soaked in TBS for 336 h.

Figure 6: SEM images of the glasses after soaked in TBS for 336h. (a) 0Sr, (b) 25Sr, (c) 50Sr, (d) 75Sr and (e) 100Sr.

Figure 7: (a) FT-IR spectra and (b) XRD patterns of the glasses after soaked in SBF for 336 h. SEM images of the glasses after soaked in SBF for 336h. (c) 0Sr, (d) 25Sr, (e) 50Sr, (f) 75Sr and (g) 100Sr.

Table 1: Nominal and analyzed compositions of the glasses and sample codes. The glass powders dissolved in 2M HNO_3 and measured compositions by ICP-OES. The analyzed compositions are shown in round brackets with standard deviation.

Table 2: The analyzed compositions of 100Sr, $100Sr_{needle\text{-}like}$ and $100Sr_{glassy}$ with

standard deviation.

Figures

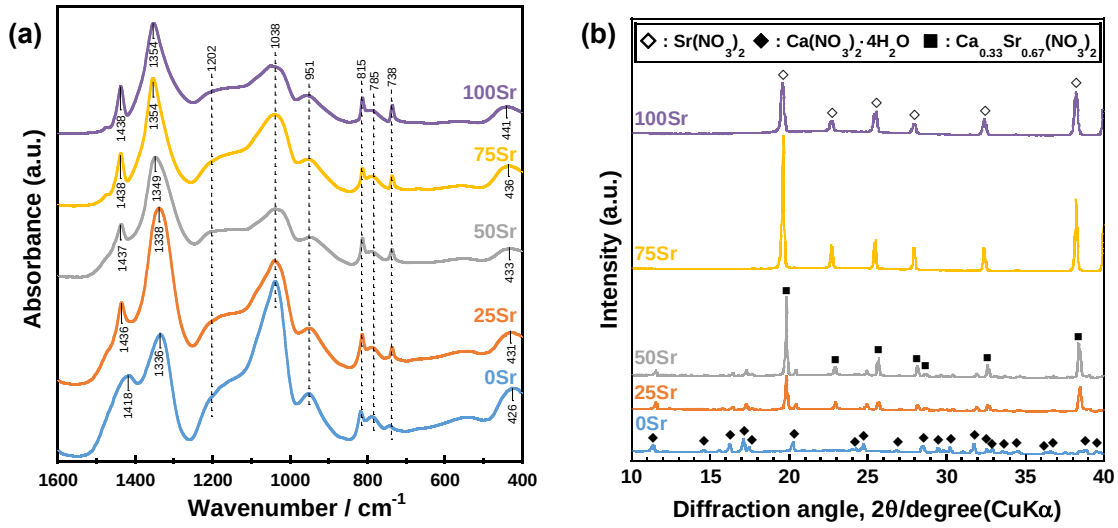

Fig. 1

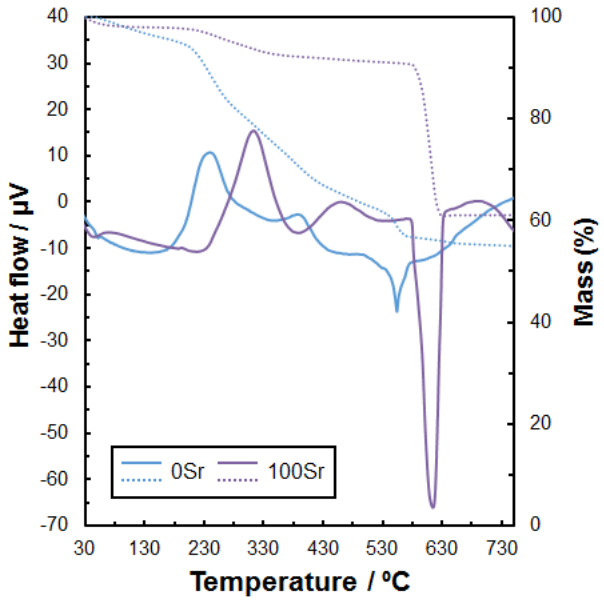
Heat flow / µV
Mass (%)
Temperature / ºC
0Sr
100Sr
40
30
20
10
0
-10
-20
-30
-40
-50
-60
-70
100
80
60
40
20
0
30
130
230
330
430
530
630
730

Fig. 2

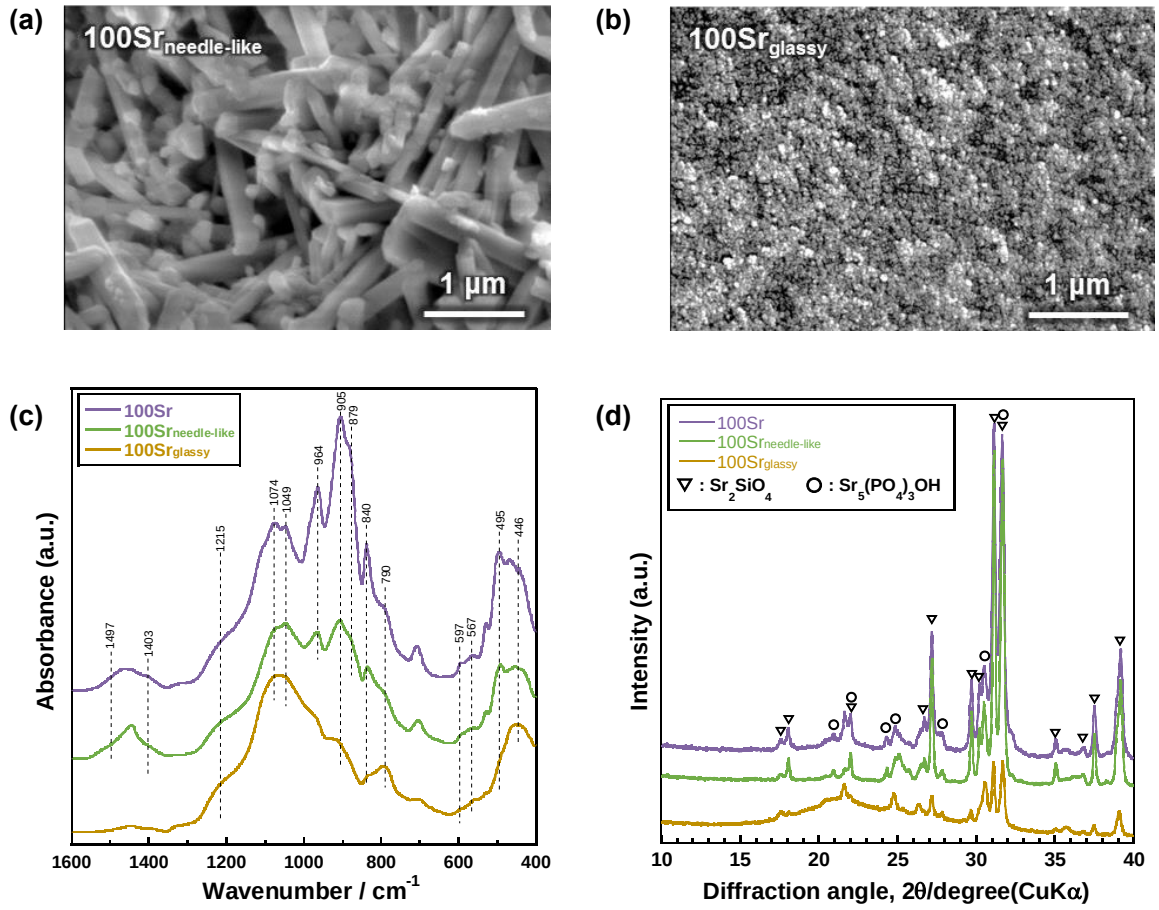
(a)
100Sr needle-like
1 μm
(b)
100Sr glassy
1 μm
(c)
100Sr
100Sr needle-like
100Sr glassy
Absorbance (a.u.)
1497
1403
1215
1074
1049
964
905
879
840
790
597
567
495
446
1600
1400
1200
1000
800
600
400
Wavenumber / cm-1
(d)
100Sr
100Sr needle-like
100Sr glassy
▽ : Sr2SiO4
○ : Sr5(PO4)3OH
Intensity (a.u.)
10
15
20
25
30
35
40
Diffraction angle, 2θ/degree(CuKα)

Fig. 3

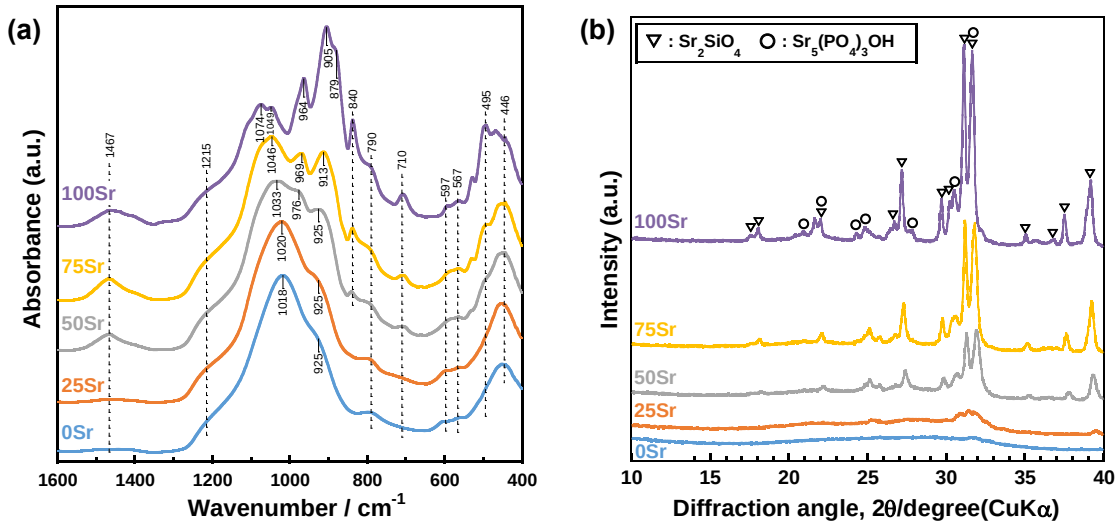
(a)
Absorbance (a.u.)
Wavenumber / cm-1
1600
1400
1200
1000
800
600
400
100Sr
75Sr
50Sr
25Sr
0Sr
1467
1215
1074
1049
1046
1033
1020
1018
964
969
976
925
925
925
905
879
840
790
710
597
567
495
446
913
(b)
▽ : Sr2SiO4 ○ : Sr5(PO4)3OH
Intensity (a.u.)
Diffraction angle, 2θ/degree(CuKα)
10
15
20
25
30
35
40
100Sr
75Sr
50Sr
25Sr
0Sr

Fig. 4

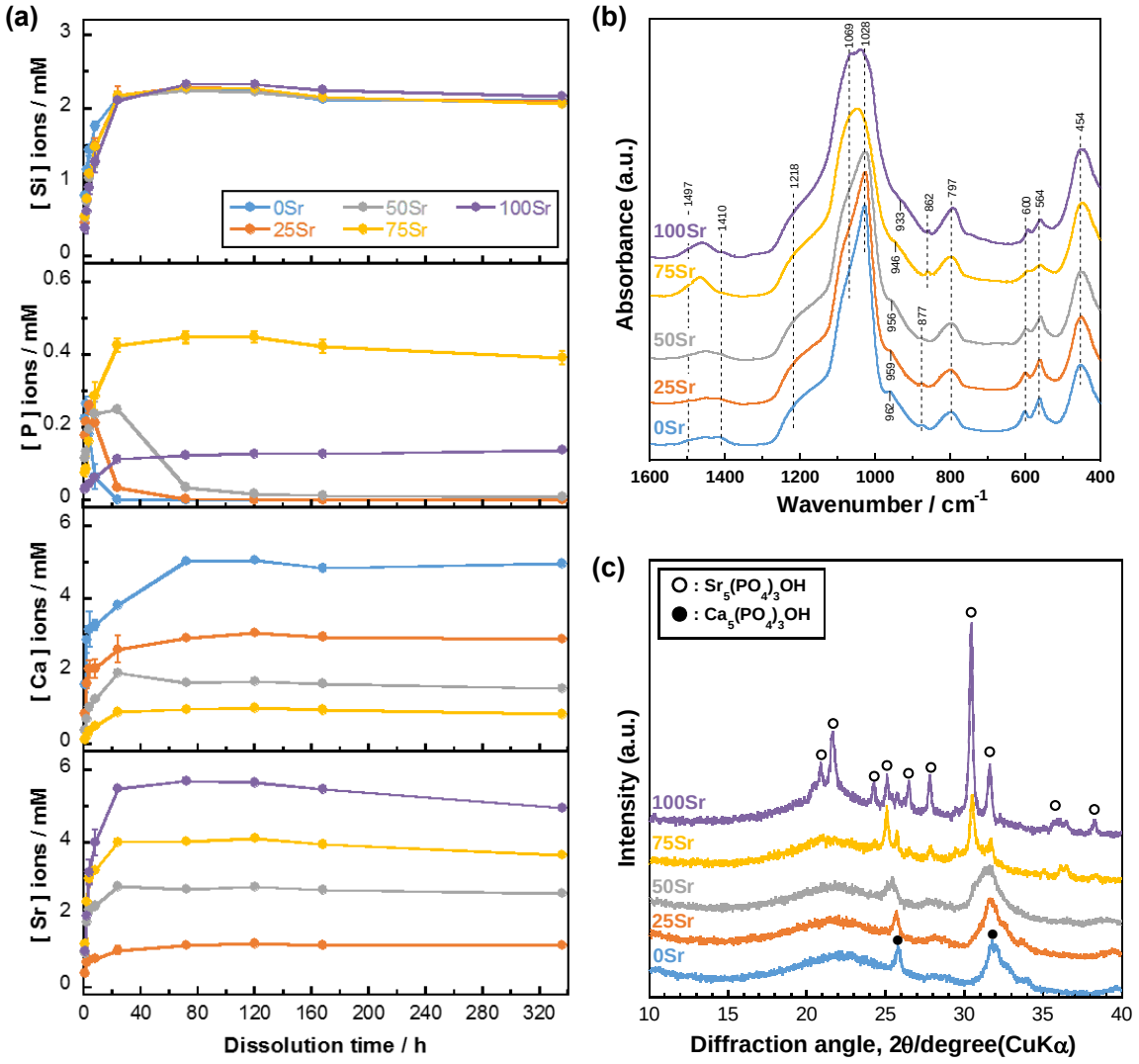
(a)
[Si] ions / mM
[P] ions / mM
[Ca] ions / mM
[Sr] ions / mM
0Sr
25Sr
50Sr
75Sr
100Sr
Dissolution time / h
(b)
Absorbance (a.u.)
Wavenumber / cm-1
1069
1028
1497
1410
1218
933
862
797
600
564
454
946
956
877
959
962
(c)
O : Sr5(PO4)3OH
● : Ca5(PO4)3OH
Intensity (a.u.)
Diffraction angle, 2θ/degree(CuKα)

Fig. 5

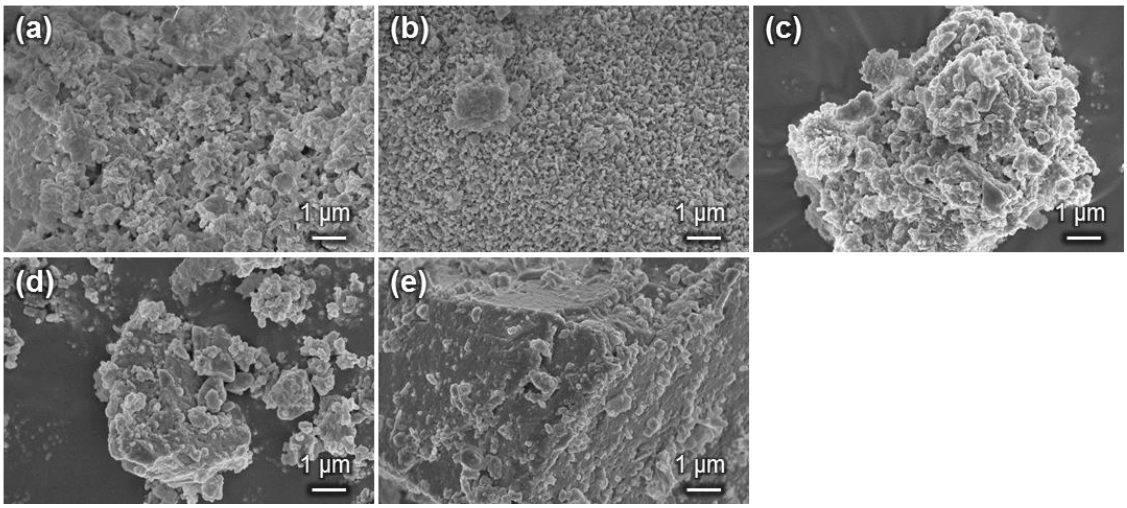

Fig. 6

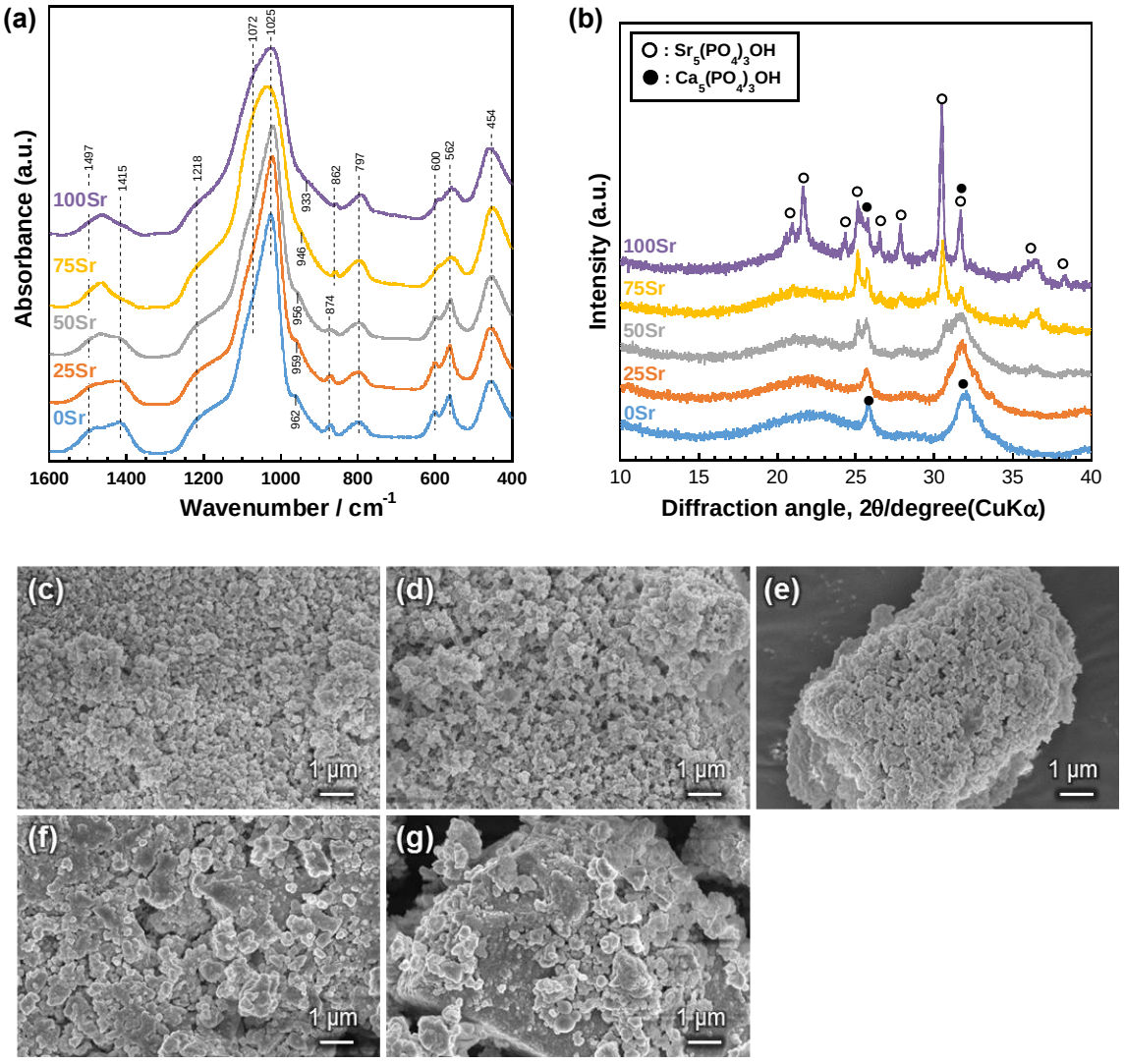
(a)
Absorbance (a.u.)
Wavenumber / cm-1
1600
1400
1200
1000
800
600
400
1497
1415
1218
1072
1025
933
946
956
959
962
874
862
797
600
562
454
100Sr
75Sr
50Sr
25Sr
0Sr
(b)
O : Sr5(PO4)3OH
● : Ca5(PO4)3OH
Intensity (a.u.)
Diffraction angle, 2θ/degree(CuKα)
10
15
20
25
30
35
40
100Sr
75Sr
50Sr
25Sr
0Sr
(c)
(d)
(e)
(f)
(g)
1 μm

Fig. 7

Tables

Table 1

Sample code	Composition (mol%)			
	SiO_2	P_2O_5	CaO	SrO
0Sr	60	4	36	-
	(61.0 ± 0.6)	(4.0 ± 0.0)	(35.0 ± 0.6)	-
25Sr	60	4	27	9
	(61.7 ± 0.4)	(4.3 ± 0.0)	(26.5 ± 0.3)	(7.5 ± 0.1)
50Sr	60	4	18	18
	(59.5 ± 0.6)	(4.1 ± 0.0)	(17.7 ± 0.3)	(18.7 ± 0.3)
75Sr	60	4	9	27
	(57.8 ± 0.2)	(4.1 ± 0.0)	(9.1 ± 0.0)	(29.0 ± 0.5)
100Sr	60	4	-	36
	(55.0 ± 0.7)	(3.8 ± 0.0)	-	(41.2 ± 0.5)

Table 2

Sample Code	Composition (mol%)		
	SiO_2	P_2O_5	SrO
100Sr	55.0±0.7	3.8±0.0	41.2±0.5
$100Sr_{needle\text{-}like}$	42.7±0.5	5.4±0.0	51.9±0.8
$100Sr_{glassy}$	75.6±0.8	9.8±0.1	14.6±0.1